Astron. Astrophys. 350, 399–413 (1999)

ASTRONOMY AND ASTROPHYSICS

Multicolor photometric properties of six early-type galaxies⋆

M.F. Saraiva, F. Ferrari, and M.G. Pastoriza

Departamento de Astronomia, Instituto de Física, Universidade Federal do Rio Grande do Sul, Av. Bento Gonçalves, 9500 – C.P. 15051, 91501-970, Porto Alegre, RS – Brazil

Received 2 March 1999 / Accepted 19 July 1999

Abstract. We present $BVRI$ CCD surface photometry for 4 elliptical and 2 S0 galaxies that show bright emission lines in their nuclear spectra. We obtained isophote maps, luminosity profiles, and basic photometric parameters. We also obtained continuum subtracted Hα+[NII] images for 5 galaxies in our sample, but only in two of them, NGC 6858 and ESO 185-54, we detected emission gas. We used the standard technique of ellipse fitting to determine the radial variation of surface brightness, color, ellipticity, position angle and the fourth order Fourier coefficient of the deviations from elliptical shape to look for isophotal twists, color gradients and fine structure variations. We have fitted an $r^{1/n}$ Sérsic law to the light profiles, finding that it provides a better fit to the light profiles of the ellipticals than the traditional $r^{1/4}$ law. However, this law does not provide a good fit for SO galaxies.

Key words: galaxies: elliptical and lenticular, cD – galaxies: photometry – galaxies: structure

1. Introduction

During the last two decades, several studies of early-type galaxies led astronomers to revise their picture of these objects, thought until the mid Seventies to be simple stellar systems, consisting of an ensemble of stars arranged in an oblate spheroid flattened by rotation, totally deprived of gas or dust.

It is now well established that elliptical galaxies are not supported by rotation, but by anisotropies in their velocity dispersion, implying they might be triaxial or prolate. The observation that in many of these objects the major axis of the isophotes rotates with increasing radius provided the evidence for triaxiality which can be intrinsic or originating in close encounters (Kormendy & Djorgovsky 1989, Capaccioli & Longo 1994)

A more recent result is that the surface luminosity profile frequently deviates from the "universal" $r^{1/4}$ law, and could in fact show a variety of shapes. Among these, the Sérsic law $r^{1/n}$ has provided the best fit in many instances (Caon et al. 1993). The parameter n takes values typically between 1 and 6, and is related to the effective radius and to the absolute magnitude of the galaxy (e.g. Prugniel & Simien 1997).

Surface photometry provides the isophote maps and the brightness profiles necessary for a better understanding of the shapes and luminosity distribution of elliptical galaxies. Other important issues that can be addressed by multicolor surface photometry are color and color gradients, which give us information about the metallicity and mean age of the stellar population. Although much smaller than in spiral galaxies, systematic color gradients have been found in early type galaxies (Prugniel & Herardeau 1998). These color gradients, as well as the integrated colors, depend on the absolute magnitude.

Multicolor photometry has been used for the detection of the interstellar medium in galaxies. Optical surveys have shown that more than 70% of the early type galaxies contain ionized gas (Goudfrooij et al. 1994, Macchetto et al. 1996) and many also contain dust (Ferrari et al. 1999). The origin of the radiation that ionizes the gas and heats the dust is not well established. One very plausible mechanism is the radiation from post-AGB stars (Macchetto et al. 1996, Ferrari et al. 1999), but photoionization by hot young stars, or nonstellar radiation, cannot be discarded.

In this paper we present $BVRI$ CCD photometry of six bright early-type galaxies, selected from a sample of 80 early-type galaxies listed in the SSRS (da Costa et al. 1988) as showing emission lines in their spectra, which we observed to obtain photometric parameters, such as isophotal shapes and colors, that can give information on their basic properties and structure. As a secondary objective we wanted to contribute to the available multicolor photometric data for elliptical galaxies, that is still far from being complete.

This paper is structured as follows. In Sect. 2 we present the observations and data reduction, in Sect. 3 we present the analysis of the data, Sect. 4 discusses each galaxy separately and Sect. 5 summarizes the results.

2. Observations and data reductions

Most of the galaxies were observed in June 1992 using the TEK 1024 CCD at the 91 cm telescope of the Cerro Tololo Inter-American Observatory (CTIO). The CCD was binned 2×2, therefore the final scale of the image was 0.792 arcsec/pixel.

Send offprint requests to: M.F. Saraiva (fatima@if.ufrgs.br)

⋆ Based on observations made at Cerro Tololo Inter-American Observatory, National Optical Astronomy Observatories, operated by the Association of Universities for Research in Astronomy, Inc., under contract with the National Science Foundation, and at the Observatório do Pico dos Dias, CNPq/Laboratório Nacional de Astrofísica, Brazil.

Table 1. Basic parameters from RC3

Object	α (2000) (h m)	δ (2000) ($^\circ$, $'$)	Type	D_{25} ($''$)	R_{25}	V (km/s)	B_T (mag)	A_B (mag)	D (Mpc)
(1)	(2)	(3)	(4)	(5)	(6)	(7)	(8)	(9)	(10)
NGC 6849	20 6.3	-40 11.8	SB0$^-$	112	1.66	5910	13.00	0.07	74
NGC 6851	20 3.5	-48 17.0	E:	122	1.38	2895	12.69	0.17	36
NGC 6958	20 48.7	-37 59.8	E+	128	1.25	2557	12.33	0.10	32
IC 4956	20 11.5	-45 35.5	E0:	102	1.04	5000	13.40	-	63
IC 4991	20 18.4	-41 3.0	S(r)0?pec	154	1.44	5518	11.56 V	0.16	69
ESO 185-54	20 3.4	-55 51.8	E2	212	1.48	4176	11.30 V	0.15	52

Description of columns:
(1) name of the galaxy
(2),(3) position (2000 coordinates)
(4) morphological type from RC3. But in ESO-LV NGC 6849 is classified as E, and NGC 6958 as E-S0.
(5) apparent major isophotal diameter at surface brightness level μ_B = 25 $\mathrm{mag\,arcsec^{-2}}$.
(6) ratio between the major and minor apparent major isophotal diameters at surface brightness level μ_B = 25$\mathrm{mag\,arcsec^{-2}}$
(7) mean radial velocity V_{GSR} in RC3 corrected for a dipole Virgo-centric flow following Tammann & Sandage (1985)
(8) total magnitude in the B system. It is followed by a "V" when it is a V-band magnitude.
(9) Galactic extinction in B magnitudes (A_g in RC3)
(10) distance from V in Column 7, assuming a Hubble constant of 80 $\mathrm{km/(s\,Mpc)}$

Table 2. Observations.

Object	scale ($''$/pix)	FWHM (B) ($''$)	Exposure time (sec) B	V	R	I	Hλ6649	Hλ6477
NGC 6849	0.792	2.0	1800	1400	400	400	3000	3000
NGC 6851	0.567	1.6	2400	2400	900	1200	-	-
NGC 6958	0.792	3.0	1200	240	120	120	1200	1200
IC 4956	0.792	2.0	1800	400	180	360	650	900
IC 4991	0.792	2.0	2400	600	150	400	900	2400
ESO 185-54	0.792	2.0	2400	600	300	450	2400	2400

The filters used were B, V, R, and I, and two narrow filters 75 Å wide centered at 6649 Å (to isolate the Hα+[NII] emission line at the red-shift of the galaxy) and at 6477 Å (to isolate a nearby region of stellar continuum). The phase of the moon was around 10 days, thus some of the galaxies were observed with bright sky. The seeing was in the range 1.7–2.8$''$.

One galaxy (NGC 6851) was observed in July 1992 using a EEV P8603A CCD at the 1.60 m telescope of the Observatório do Pico dos Dias - Laboratório Nacional de Astrofísica, Brazil (OPD), also with B, V, R, and I filters. The final scale of the corresponding images was 0.567 arcsec/pixel. The phase of the moon was new, and the seeing was typically 1.7 $''$. For all program galaxies, at least two exposures were obtained in each band. Multiple exposures of standard stars from Graham (1982) were also obtained for the photometric calibration. The observation log is shown in Table 2.

2.1. Reduction of the $BVRI$ images

The images were corrected for bias and flat-field using standard IRAF[1] routines, and the multiple exposures in each filter were then combined. The sky background for each broad-band image was determined with the IRAF routine `imsurfit`, by fitting a 2nd order polynomial to the frame regions around the galaxy, after removing all the stars in the frames. The uncertainties in the sky background, including local fluctuations and deviations from the mean, were 0.007 magnitudes on average for the $BVRI$ filters for the frames taken with moon light, [$\mu_V(sky) \simeq 19\ \mathrm{mag\,arcsec^{-2}}$], and 0.015 for the frames taken without moon light [$\mu_V(sky) \simeq 21\ \mathrm{mag\,arcsec^{-2}}$].

The photometric calibration of the data to the Johnson-Cousins system was made using observations of standard stars in the E-Regions (Graham 1982); 10 stars were used in the observations at CTIO, and 6 stars were used in the observations at OPD.

The transformation equations between the standard magnitudes and colors (upper case), and the instrumental magnitudes and color corrected for atmospheric extinction (lower case), for the CTIO observations, were:

$$B - V = (1.26 \pm 0.016)(b - v)_o - (0.45 \pm 0.017)$$
$$V = v_o - (0.03 \pm 0.009)(B - V) + (22.58 \pm 0.008)$$

[1] IRAF - Image Reduction and Analysis Facility - is distributed by the National Optical Astronomy Observatories, which is operated by the Association of Research in Astronomy, Inc., under cooperative agreement with the National Science Foundation, USA

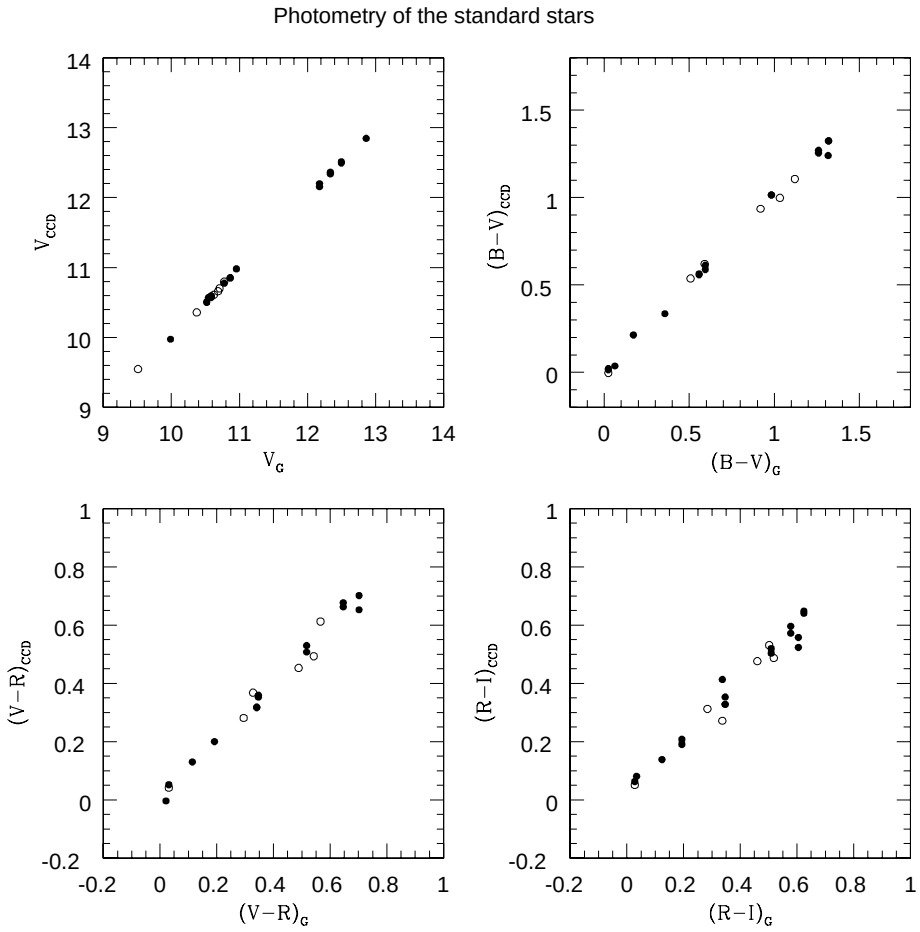

Fig. 1. Comparison between our CCD photometry of the standard stars (vertical axes) and the photometry of Graham (horizontal axes). The solid dots represent the stars of the CTIO run, and de circles represent the stars of the OPD run.

$$V - R = (0.96 \pm 0.023)(v - r)_o - (0.07 \pm 0.012)$$
$$R - I = (0.99 \pm 0.042)(r - i)_o + (0.68 \pm 0.016)$$

and for the OPD observations were:

$$B - V = (1.51 \pm 0.04)(b - v)_o - (1.53 \pm 0.06)$$
$$V = v_o - (0.05 \pm 0.03)(B - V) + (20.58 \pm 0.02)$$
$$V - R = (0.86 \pm 0.05)(v - r)_o - (0.29 \pm 0.05)$$
$$R - I = (0.85 \pm 0.07)(r - i)_o + (0.90 \pm 0.05)$$

A comparison between our CCD photometry of the standard stars calibrated to the Johnson-Cousin system through the above equations, and Graham's photometry, is shown is Fig. 1.

As a check of our calibration, we compared the magnitudes and colors of the galaxies obtained with the transformation equations, with the available aperture photometry of the galaxies. In some cases it was necessary to do a transformation of the compiled R and I aperture photometry to the Cousin system. For all the galaxies that had available aperture photometry, we found some magnitude and color differences between the photoelectric photometry and the calibrated CCD photometry. The zero points of the transformation equations were then adjusted to fit the photoelectric photometry of the galaxies. In the case of galaxies that had no photoelectric photometry, we maintained the zero points of the transformation equations. The mean differences between the zero points from the standard stars only (SS), and zero points adjusted to photoelectric photometry (PP) were, for the CTIO data:

$$\langle B - V\rangle_{\rm PP} - \langle B - V\rangle_{\rm SS} = 0.05 \pm 0.04 \quad (N = 64)$$
$$\langle V\rangle_{\rm PP} - \langle V\rangle_{\rm SS} = 0.06 \pm 0.03 \quad (N = 43)$$
$$\langle V - R\rangle_{\rm PP} - \langle V - R\rangle_{\rm SS} = -0.00 \pm 0.03 \quad (N = 31)$$
$$\langle R - I\rangle_{\rm PP} - \langle R - I\rangle_{\rm SS} = -0.05 \pm 0.13 \quad (N = 16)$$

and for the OPD data:

$$\langle B - V\rangle_{\rm PP} - \langle B - V\rangle_{\rm SS} = -0.28 \pm 0.03 \quad (N = 9)$$
$$\langle V\rangle_{\rm PP} - \langle V\rangle_{\rm SS} = 0.08 \pm 0.03 \quad (N = 10)$$
$$\langle V - R\rangle_{\rm PP} - \langle V - R\rangle_{\rm SS} = 0.20 \pm 0.02 \quad (N = 8)$$
$$\langle R - I\rangle_{\rm PP} - \langle R - I\rangle_{\rm SS} = -0.13 \pm 0.04 \quad (N = 5)$$

where N is the number of apertures compared.

Fig. 2 shows the comparison between our CCD photometry calibrated to the Johnson-Cousin system, after the zero point shift, and the photoelectric photometry for the four galaxies for which photoelectric photometry was available in all the $BVRI$ passbands.

2.2. Emission line images

The images were corrected for bias and flat-field in the same way as for the broad-band images, and the multiple exposures in each

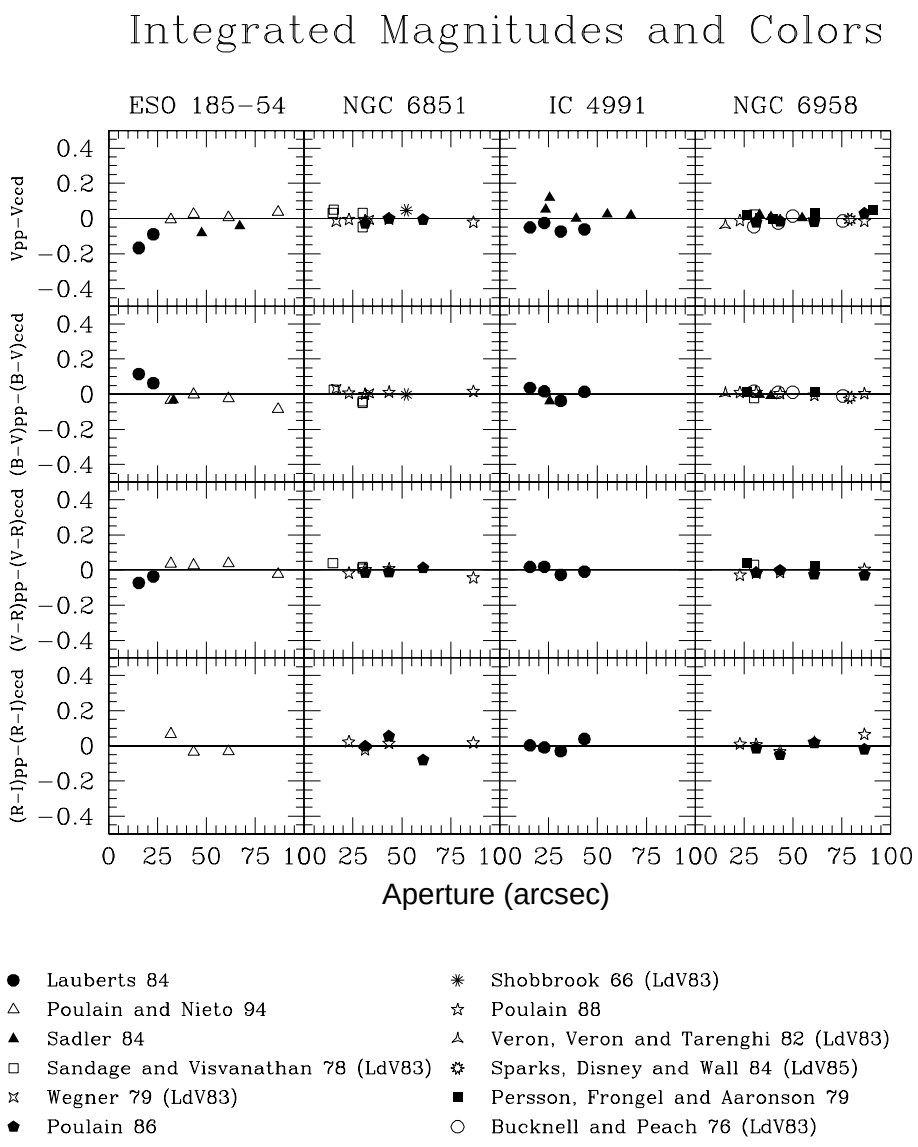

Fig. 2. Comparison between our CCD photometry calibrated to the Johnson-Cousin system (solid dots) and the available photoelectric photometry in the same system (symbols explained in the legend). Only the four galaxies that have photoelectric photometry in the four passbands are shown.

filter were combined. To obtain the final continuum subtracted Hα emission line images, we scaled the continuum image to match the intensities of the emission image using the parameters obtained from a linear regression of the mean intensity of the isophotes in both images. This procedure should result in a continuum subtracted image with average zero intensity where there is no gas emission.

Only for two objects, NGC 6958 and ESO 185-54, we found a significant number of counts in the central region above a threshold of two times the rms value of the background.

To compute the Hα+[NII] fluxes, we have converted the measured counts into an absolute flux scale using Eq. (5) in Macchetto et al. (1996). In our case, the parameter ϵ in that equation is ϵ =1, since we have used a narrow filter centered at λ = 6477 Å to isolate and subtract the continuum.

The Hα+[NII] flux for NGC 6958, measured above a threshold of sensitivity of $1\,10^{-17}\,\mathrm{ergs\,s^{-1}\,cm^{-2}\,arcsec^{-2}}$, was estimated as $2\,10^{-14}\,ergs\,s^{-1}\,cm^{-2}$, corresponding to an H$\alpha$+[NII] luminosity of $2\,10^{39}\,ergs\,s^{-1}$. For ESO 185-54 the threshold sensitivity was $6\,10^{-18}\,\mathrm{ergs\,s^{-1}\,cm^{-2}\,''^{-2}}$, the H$\alpha$+[NII] flux was $1\,10^{-15}\,\mathrm{ergs\,s^{-1}\,cm^{-2}}$, and the corresponding Hα+[NII] luminosity was $4\,10^{38}\,ergs\,s^{-1}$.

These values are in the lower limit of the range of Hα+[NII] luminosities calculated by Macchetto et al. (1996) for a large sample of early-type galaxies.

3. Analysis

3.1. Isophote maps and ellipse fits

R band isophote maps of the sample galaxies are shown in Fig. 3, after removing all the background stars, except the stars superimposed on to the galaxies. As expected for early-type galaxies, the isophotes have shapes that resemble more or less elongated ellipses, some more pointed, others more squared. The main reason for the shape variations is a simple consequence of inclination, but some of them cannot arise from inclination effects, and are supposed to be indications of intrinsic features,

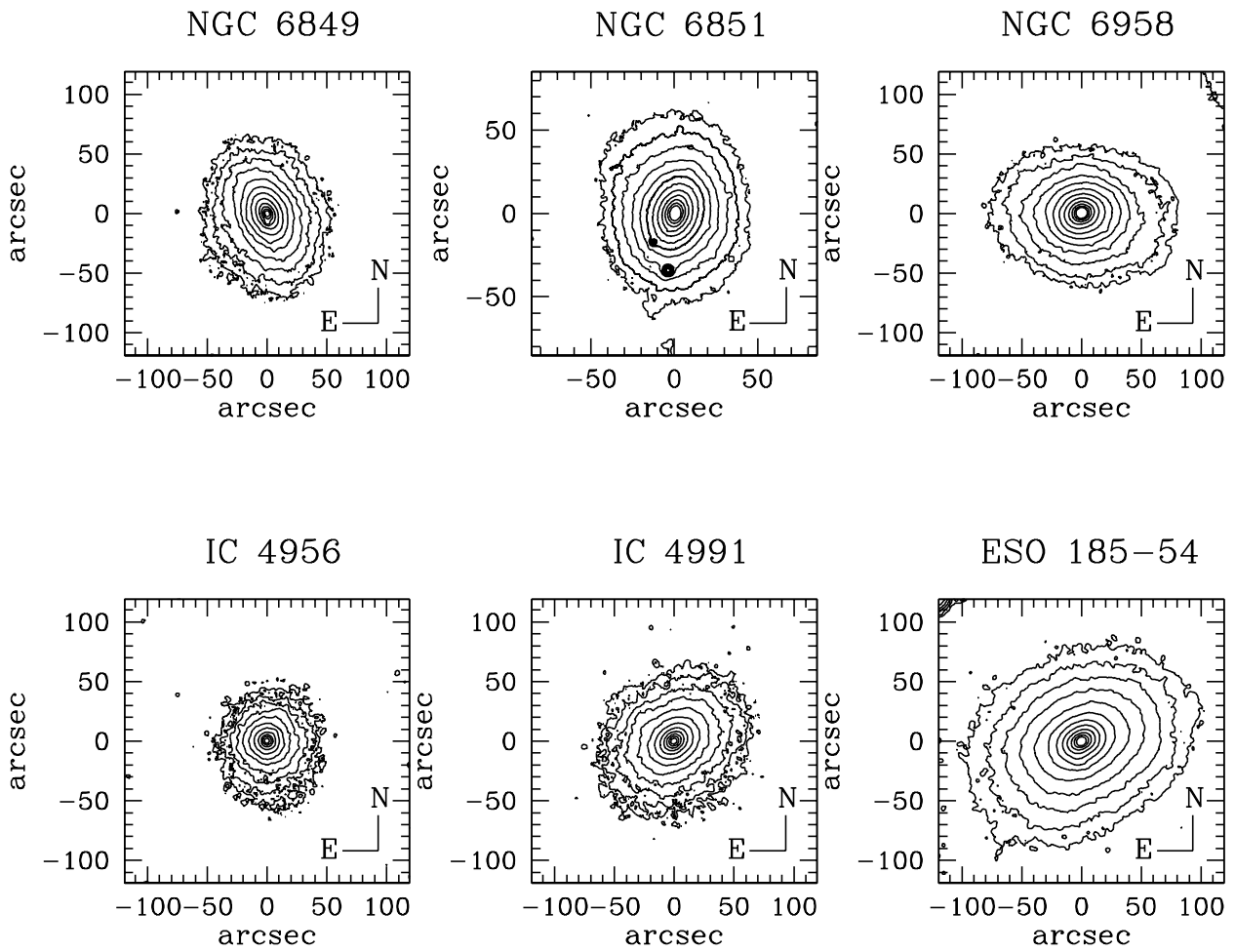

Fig. 3. Isophote maps of the sample galaxies in the R band. Isophote levels range from: **NGC 6849** μ= 18 to 24 mag arcsec^{-2}; **NGC 6851** μ= 18 to 23 mag arcsec^{-2}; **NGC 6958** μ= 18 to 23.5 mag arcsec^{-2}; **IC 4956** μ= 18 to 23 mag arcsec^{-2}; **IC 4991** μ= 18 to 23.5 mag arcsec^{-2}; **ESO 185-54** μ= 18 to 23.5 mag arcsec^{-2}. The differences between successive levels were 0.5 mag arcsec^{-2} in all the maps.

such as triaxiality (Bertola 1981), or gravitational interaction (Binney & Petrou 1985).

To quantify these differences, we have used the task `ellipse` in the STSDAS package for IRAF, fitting ellipse to the B, V, R, and I isophotes. Our principal interest was to determine the position angle (PA) of the isophotes, their ellipticity (ϵ), and the Fourier amplitudes of deviations from perfect ellipticity ($\cos 4\theta$ term, $B4$), as well as the the average brightness along the isophotes. The behavior of the position angle is an indicator of shape because, if the galaxies are spheroidal, irrespective of the inclination, the semi-major axis will keep the same direction (Mihalas & Binney, 1981). This implies that, if the position angle rotates, the galaxy is probably triaxial. Another possible origin of isophotal twist is interaction with another galaxy (Bender & Möllenhoff 1987). The behavior of ellipticity in different wavebands is an indicator of dust, since in the presence of dust the blue light will be more absorbed than the red light - the blue isophotes will be more distorted than the red ones. The Fourier term $B4$ is an indicator of the presence of subsystems, as $B4 > 0$ indicates "disky" isophotes, i.e., isophotes more pointed than pure ellipses, and $B4 < 0$ indicates "boxy" isophotes, i.e, isophotes more rectangular than pure ellipses (Jedrzejewski, Davies & Illingworth 1987). Bender & Mölennhoff (1987) found that "disky" isophotes are associated with the presence of a disky subsystem intrinsic to the galaxy, whereas boxy isophotes tend to appear in massive elliptical galaxies, and might be an indication of interaction. Finally, the average brightness along the isophotes gives the luminosity distribution in the galaxy, presumably associated with the mass distribution. By combining different filters, we can derive the color and therefore the type of stars that produce the observed luminosity.

Fig. 4 shows the variation of the ellipticity, position angle and $\cos 4\theta$ term ($B4$), with the 1/4 power of the ellipse semi-major axis ($a^{1/4}$). The uncertainties were obtained directly from the rms scatter of intensity data along the fitted ellipse. The variation of the isophotal brightness and color indices with $a^{1/4}$ are displayed in Fig. 5, as well as the error bars in each level due to the uncertainty in the sky subtraction. The uncertainties in surface brightness were calculated as:

$$d\mu \;=\; 1.0857\,\frac{d\,I_{sky}}{I_{(galaxy-sky)}}$$

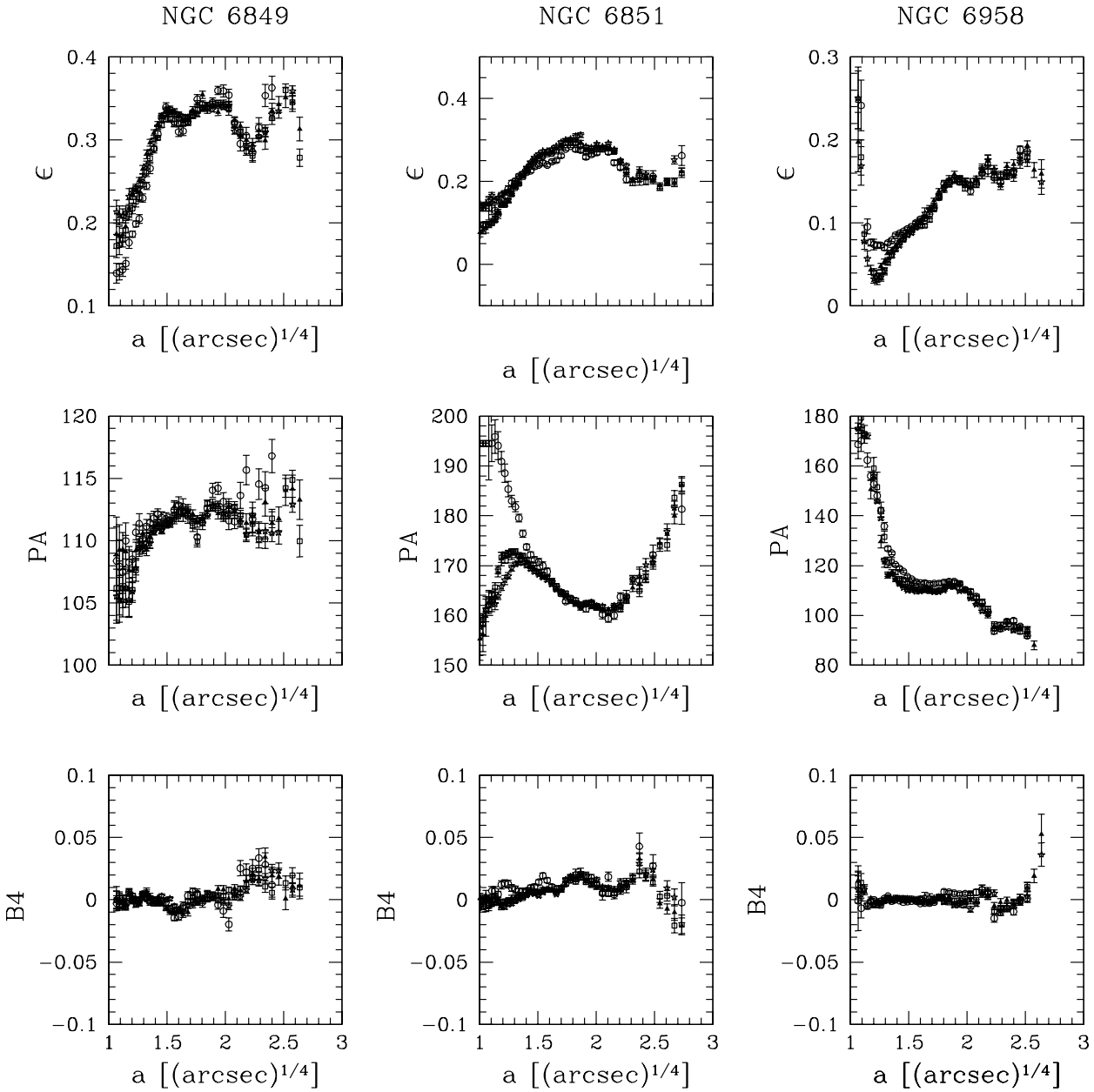

Fig. 4. Isophotal parameters ellipticity (ϵ), position angle (PA), and $\cos\ 4\theta$ Fourier term ($B4$), as a function of the ellipse fourth power of the semimajor axis ($a^{1/4}$). The symbols circles, squares, triangles, and stars represent the filters B, V, R, and I respectively.

and the uncertainties in color were calculated by adding quadratically the uncertainties in surface brightness.

3.2. Shape of the luminosity profiles

After fitting the ellipses, we re-ran the task `ellipse` keeping fixed the shape of the ellipse using the mean values of the last isophotes. In this way we obtained an elliptically averaged profile along the major axis of the galaxy, and used this profile to find the function that best describes the brightness distribution of the galaxy.

The fit was made using the task `nfit1d` in the STSDAS package, using a Sersic $r^{1/n}$ law (Sersic 1968, Ciotti 1991, Graham et al. 1998), given by the expression

$$I(r) = I_e\, 10^{-b_n\left[\left(\frac{r}{r_e}\right)^{\frac{1}{n}}-1\right]}$$

where $b_n = 0.868n - 0.142$ is such that r_e becomes the radius enclosing half of the total luminosity of the galaxy, called the effective radius, and I_e is the surface brightness along the isophote with radius r_e. For n=4 this equation is identical to the de Vaucouleurs $r^{1/4}$ law, with the same meaning of the parameters I_e and r_e. We performed the fit by allowing n, I_e and r_e to be free parameters.

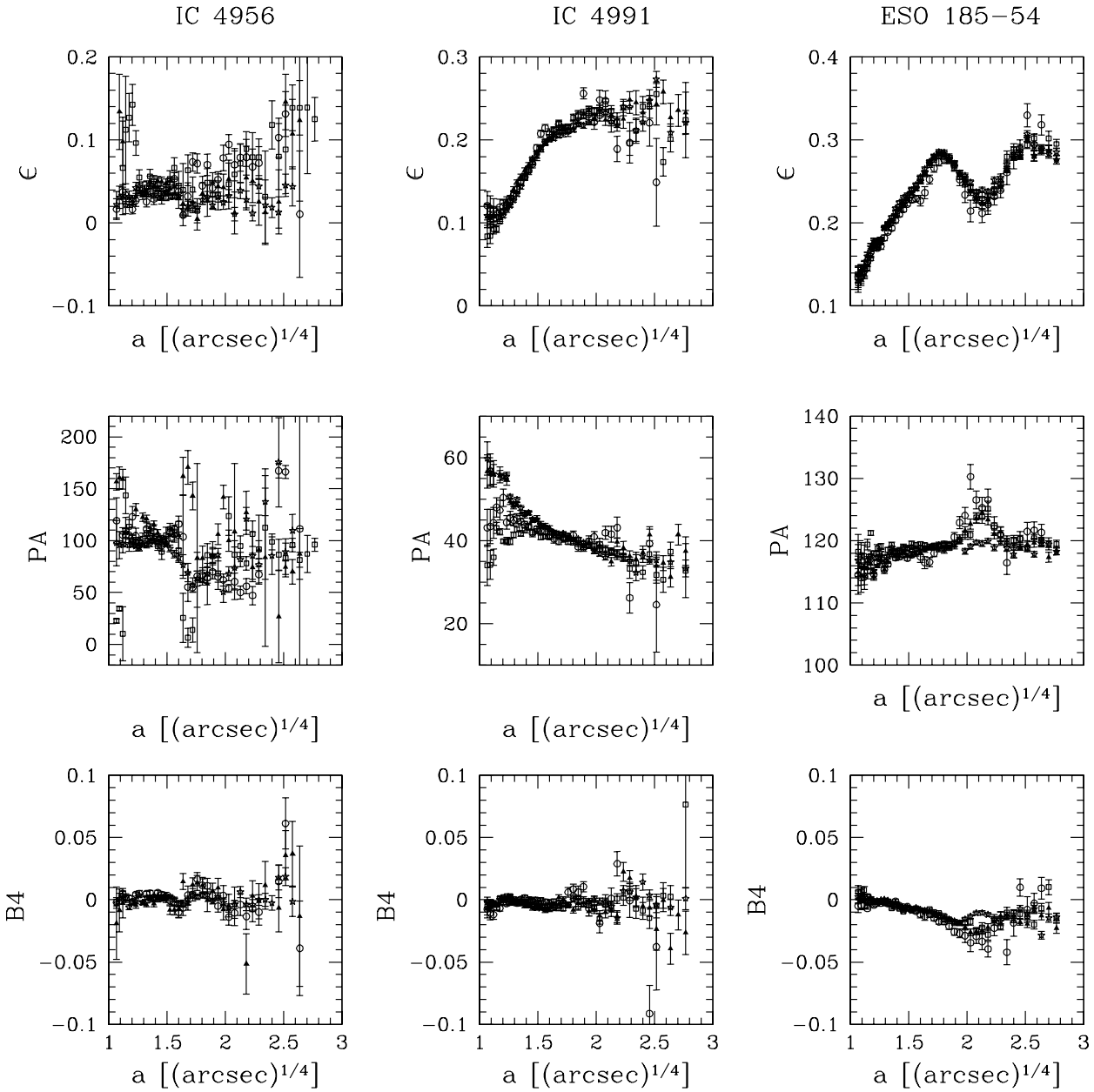

Fig. 4. (continued)

Table 3. Fit parameters with $r^{1/n}$ law

Object	Fit region [″] [μ]	n ±	$I_e[\mu]$ ±	a_e [″] ±	a_e[kpc] ±
NGC 6849	7.9–76.4	2.4	23.4	29.11	10.42
	21.1 -25.6	0.1	0.08	0.09	0.03
NGC 6851	5.6–39.7	5.0	22.05	17.18	2.99
	19.9–24.5	0.2	0.04	0.41	0.07
NGC 6958	7.0–61.0	6.8	23.5	41.9	6.5
	20.6–24.7	2.1	0.09	2.2	0.3
IC 4991[a]	5.0–76.4	6	24.85	71.22	23.7
	20.9–24.9	-	0.04	2.37	0.8
ESO 185-54	7.9–76.4	4.9	23.9	55.6	10.5
	20.2–24.6	0.3	0.16	4.5	0.8

[a] For this galaxy we had to keep n fixed

It is important to note that the final parameters depend strongly on the fitted region. In the inner part of the profile, where the points are more packed and have higher intensity values, the inclusion of one or two more points in the fitted region can change significantly the shape of the curve. In the outer part, the uncertainties are large, so the modeled profile may be a little above or below the data points and still be a probable fit. Keeping these restrictions in mind, we performed the fit by changing the initial parameters as well as the inner limit of the fitted region, until we obtained the best χ^2 provided that the fitted function did not fall above the observational points in the faint part of the profile.

For one galaxy (IC 4956), the fit with the Sérsic law was not adequate. For another (IC 4991), we had to keep n fixed

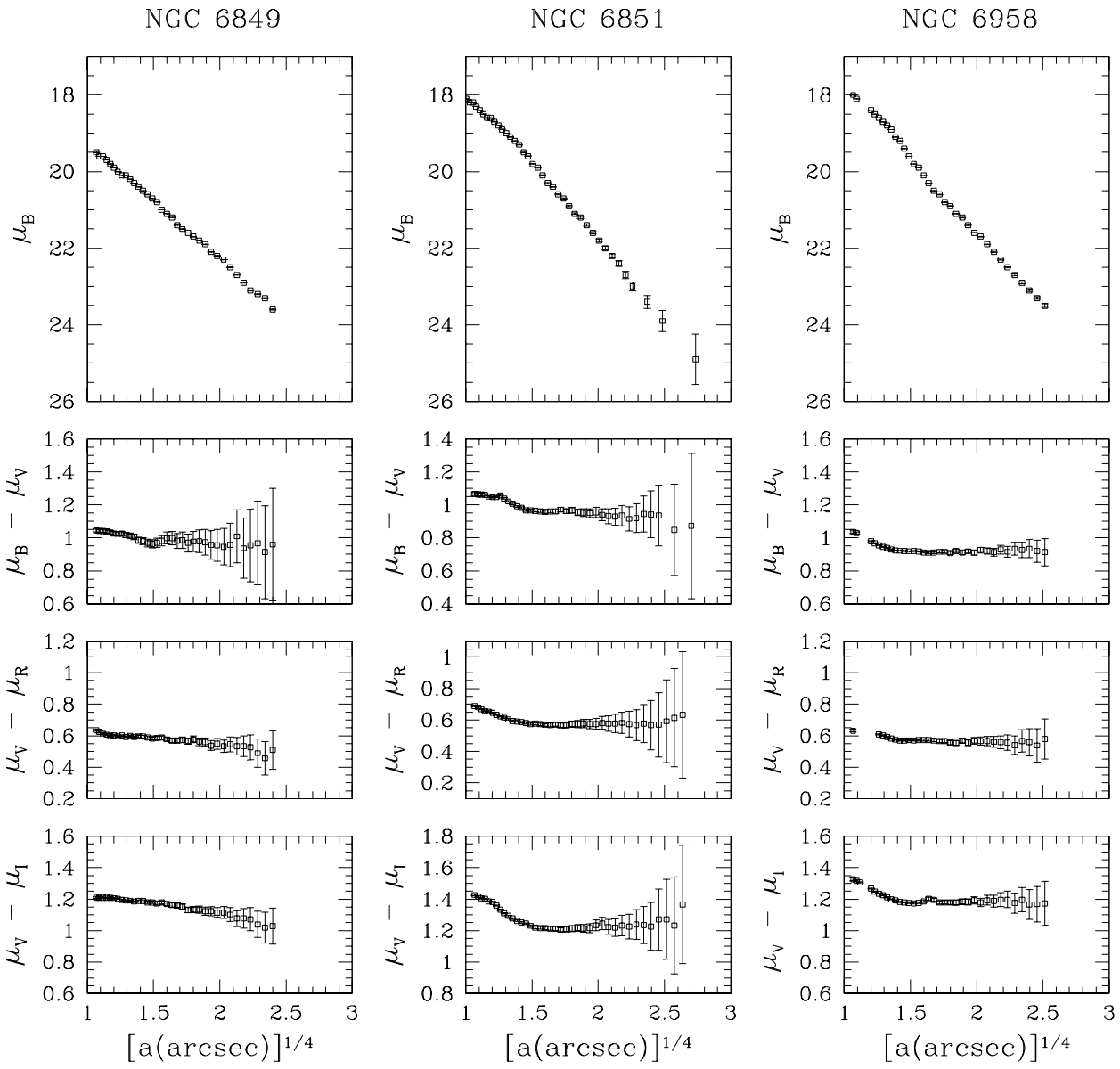

Fig. 5. Surface brightness and color indices profiles averaged over isophotes, as a function of the fourth power of the semi-major axis of the ellipse fitted to the isophote.

to prevent the fitted function from falling above the data in the outer part of the profile. For these two galaxies, we made another fit including an exponential disk in the fitting function,

$$I(r) = I_e\, 10^{-b_n\left[\left(\frac{r}{r_e}\right)^{\frac{1}{n}}-1\right]} + I_0\, e^{-\frac{r}{r_0}}$$

The final parameters, listed on Tables 3 and 4, are not the only ones that can describe the observed profiles, but the ones that best described the largest range of magnitudes (approximately four magnitudes) that we considered reliable.

The best fit for each galaxy is shown in Fig. 6. Fig. 7 shows the plots of n against the effective surface brightness, the effective semi-major axis, ellipticity, and absolute magnitude, as well as the relation between I_e and r_e. IC 4956 is not shown in the plots because it did not fit an $r^{1/n}$ function. Apparently, the correlation between the index n and the parameters μ_e and M_B, found by Caon et al. (1993) and Prugniel & Simien (1997), does not exist among the galaxies in our sample. However, the galaxies seem to be separated in two groups, one containing the three galaxies brighter than $M_B = -21$ and the other containing the two galaxies fainter than this value. Inside each group, there is an apparent correlation but our sample is far too small to provide any statistically valid result. The distinction between the two groups is not noticeable in the plot of μ_e versus re, where all the data lay very close to the relation found by Hamabe & Kormendy (1987), and also very close to the data of Capaccioli & Caon (1991) for a sample of E and S0 galaxies in the Virgo cluster brighter than $M_B = -20.9$.

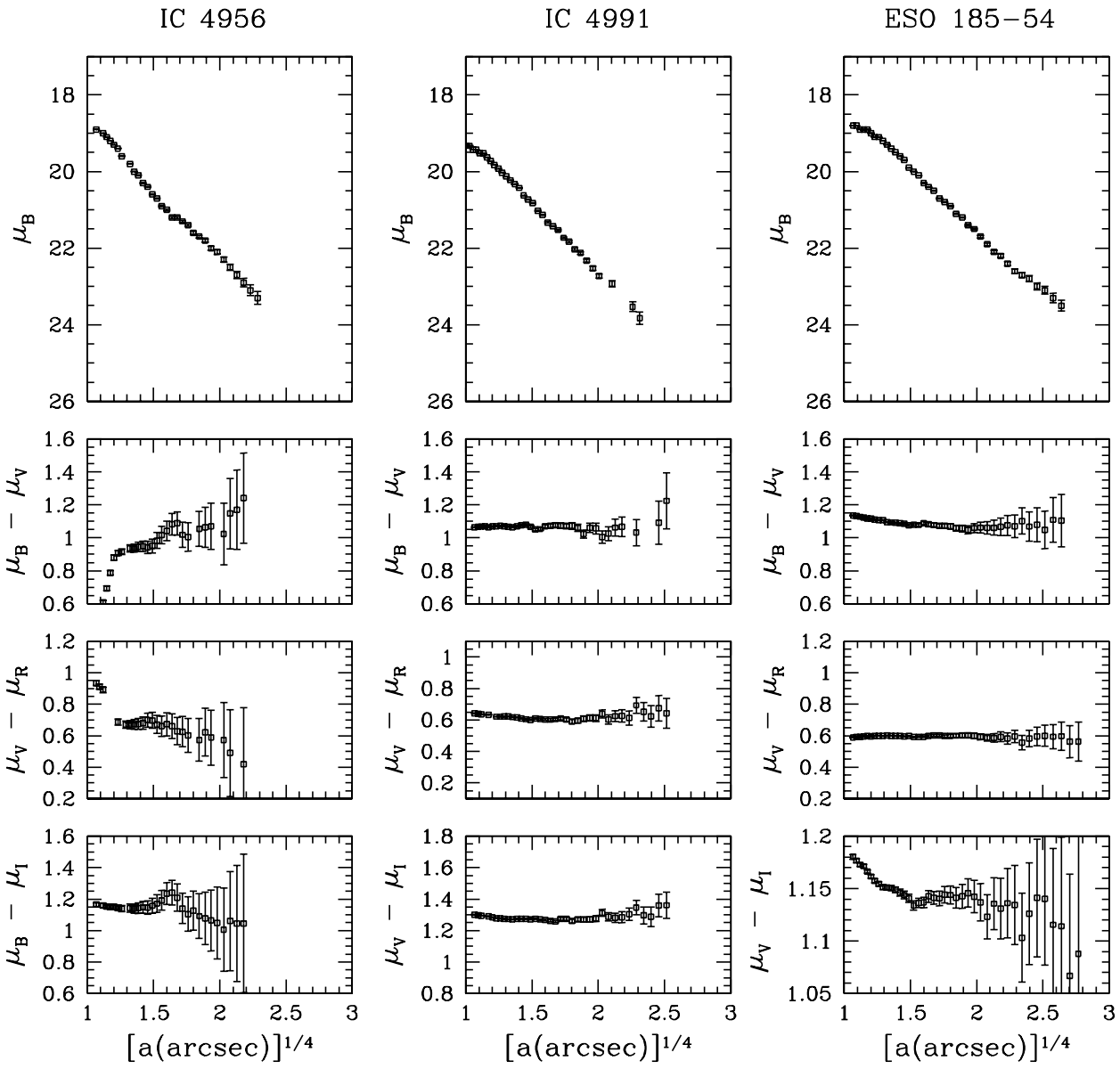

Fig. 5. (continued)

Table 4. Fit parameters with a $R^{1/n}$ law plus and exponential law

Object	Fit region [″] [μ]	n ±	I_e [μ] ±	a_e [″] ±	a_e[kpc] ±	I_0 [μ] ±	a_0 [″] ±	a_0[kpc] ±
IC 4956	3.0–38.6	0.91	20.00	2.57	0.794	20.58	10.4	3.21
	19.9–24.2	0.06	0.02	0.02	0.006	0.03	0.2	0.06
IC 4991	5.0–76.6	3.8	22.5	17	6.6	22.8	32	10.7
	20.3–24.8	0.4	0.2	2.8	1.0	0.2	2.0	0.6

3.3. Integrated photometric parameters

The B, V, R, and I integrated magnitudes and colors were obtained by integrating the light in elliptical annuli with the shape of the external isophotes. The ellipses were the same used to obtain the elliptically averaged profiles. The growth curves for magnitude and color thus obtained are shown in Fig. 8. A red gradient towards the nucleus can be seen in almost all the galaxies.

Table 5 lists the magnitudes and colors integrated up to the last ellipse for which the ellipse fitting proceeded normally. The listed uncertainties include uncertainties in the sky subtraction and in the calibration.

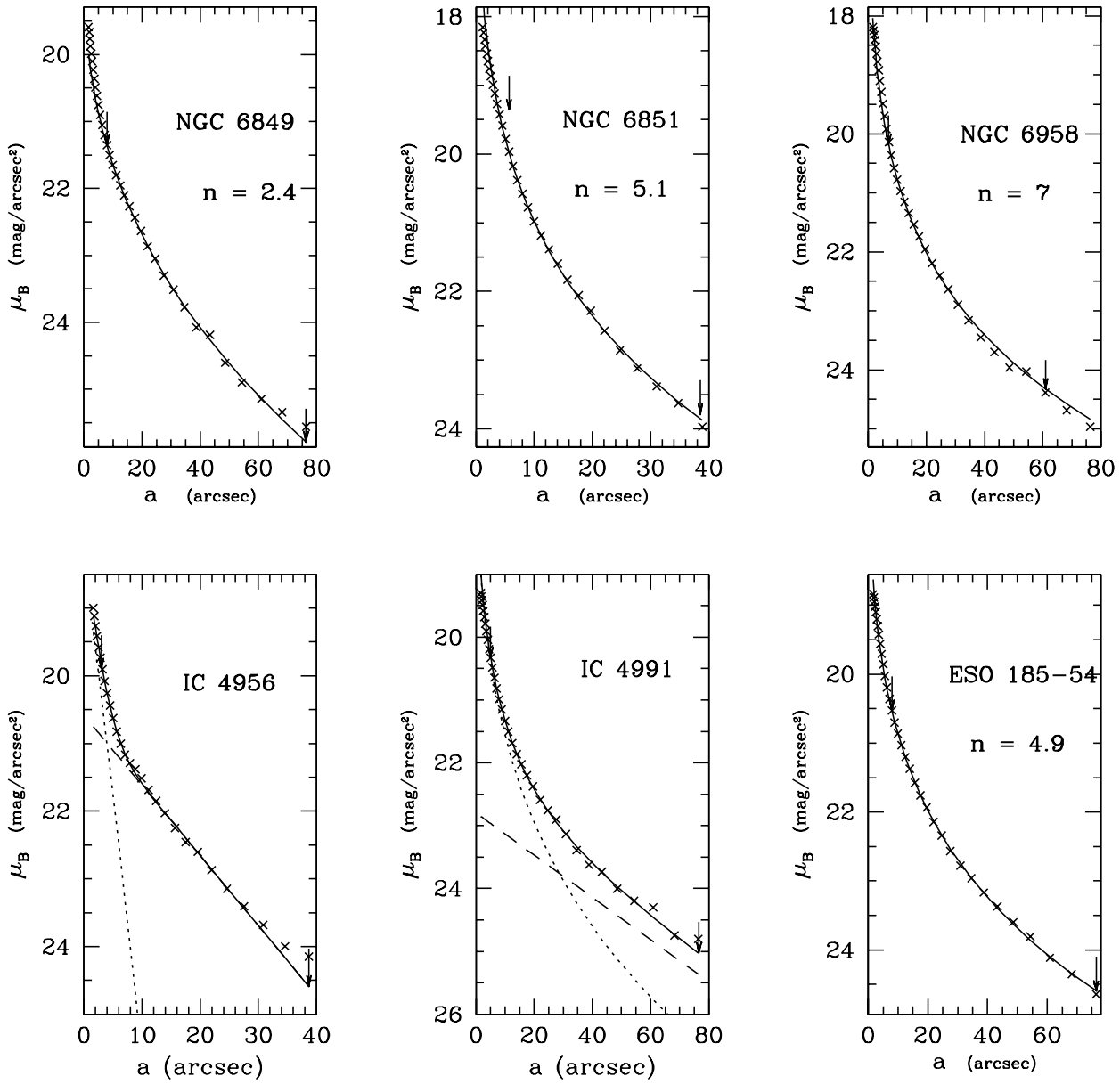

Fig. 6. Fit of the B mean surface brightness profile with and $r^{1/n}$ law. The crosses are the elliptically averaged profile, the continuous line is the fitted function. For IC 4956 and IC 4991 which fit demanded the inclusion of a disk model, the continuous line represent the sum of the disk function (dashed line) and the bulge function (dotted line). The parameters of each function are listed in Tables 3 and 4. The arrows indicate the limits of the fit regions.

The magnitudes and colors were corrected for galactic extinction, by adopting the value for the galactic extinction in the B band [$A_g(B)$] given in RC3, following the procedures of the same catalogue to calculate the color excess $E(B-V)$, and using the color excesses ratios given in Buta & Williams (1995) to calculate the color excesses $E(V-R)$ and $E(V-I)$.

To obtain the total B magnitudes, we proceeded in two ways: first, we fitted a standard growth curve taken from RC3 to the integrated magnitude curve; second, we extrapolated the elliptically averaged profile from the last ellipse to infinity by assuming the same brightness function distribution that best fitted the outer parts of the profile.

This second procedure is often inadequate, because of the large uncertainty in the photometry at these very faint light levels (Caon et al. 1993). On the other hand, the fit of the growth curves to the profiles is fairly good, as can be seen in Fig. 8. Thus, when the total magnitudes determined from the two methods differed by more than 0.15 magnitudes, we adopted the value given by the first method, otherwise we adopted the mean value from both measurements.

In Table 6 we list the extrapolated total magnitudes of the galaxies, and the corresponding absolute magnitudes. The average values of the corrected total colors of the galaxies in our sample are $\langle(B-V)^o\rangle = 0.97 \pm 0.08$, $\langle(V-R)^o\rangle = 0.54 \pm 0.03$,

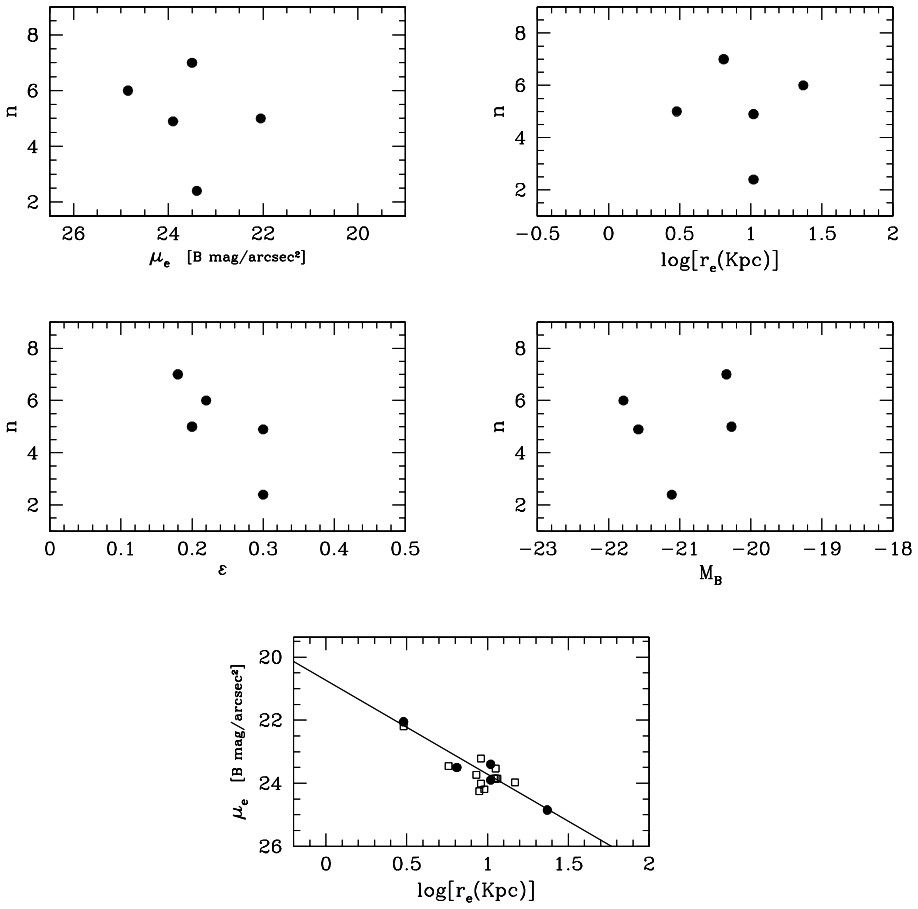

Fig. 7. Four first panels: plots of n against the global parameters μ_e, $\log(a_e[\mathrm{kpc}])$, ellipticity ϵ, and absolute magnitude M_B. Last panel: plot of μ_e versus $\log(a_e[\mathrm{kpc}])$. The continuous line is the correlation found.

Table 5. Integrated magnitudes and colors

Object	a (arcsec) a (kpc)	B B^0	$(B-V)$ $(B-V)^0$	$(V-R)$ $(V-R)^0$	$(V-I)$ $(V-I)^0$
NGC 6849	76.4	13.61 ± 0.06	1.04 ± 0.04	0.51 ± 0.04	1.18 ± 0.04
	27.4	13.33 ± 0.06	0.98 ± 0.04	0.48 ± 0.04	1.10 ± 0.04
NGC 6851	46.15	12.97± 0.06	0.91 ±0.044	0.58±0.021	1.23±0.036
	8.0	12.80± 0.06	0.84 ±0.044	0.55±0.021	1.14±0.036
NGC 6958	76.4	12.51± 0.02	0.94 ± 0.05	0.56 ± 0.05	1.19 ± 0.04
	23.6	12.41 ± 0.02	0.92 ± 0.05	0.55 ± 0.05	1.16 ± 0.04
IC 4956	38.7	13.42 ± 0.09	1.05 ± 0.06	0.55 ± 0.06	1.13 ± 0.06
	11.9	13.26 ± 0.09	1.01 ± 0.06	0.53 ± 0.06	1.03 ± 0.06
IC 4991	76.4	12.97 ± 0.06	1.01 ± 0.06	0.57 ± 0.05	1.26 ± 0.04
	25.5	12.81 ± 0.06	0.97 ± 0.06	0.55 ± 0.05	1.22 ± 0.04
ESO 185-54	76.4	12.60 ± 0.14	1.12 ± 0.08	0.58 ± 0.07	1.13 ± 0.07
	19.3	12.45 ± 0.14	1.09 ± 0.08	0.56 ± 0.07	1.09 ± 0.07

and $\langle (V-I)^o \rangle = 1.11 \pm 0.08$. These are very typical of early type galaxies if compared with the mean color computed by Prugniel & Hérardeau (1998), and by Buta & Williams (1995).

A linear fit of the color-absolute magnitude relation results in:

$$
\begin{aligned}
B-V &= (-0.10 \pm 0.04)\, M_B + (-1.1 \pm 0.9) \\
V-R &= (0.00 \pm 0.02)\, M_B + (0.6 \pm 0.5) \\
V-I &= (-0.01 \pm 0.054)\, M_B + (0.9 \pm 1.0)
\end{aligned}
$$

where we can see a small tendency of more luminous galaxies to be redder.

The nuclear colors of the galaxies are in general a little redder than the total colors. This means that the Hα+[NII] emission detected in the nuclear spectra of these galaxies (da Costa et al. 1988) cannot be caused by recent star formation in the nuclear region, since young starbursts would make the colors bluer, not redder (Bica et al. 1990). Thus we conclude that, if these galaxies do have ionized gas in their nuclei, post-AGB stars are probably the main mechanism responsible for the ionization of the gas.

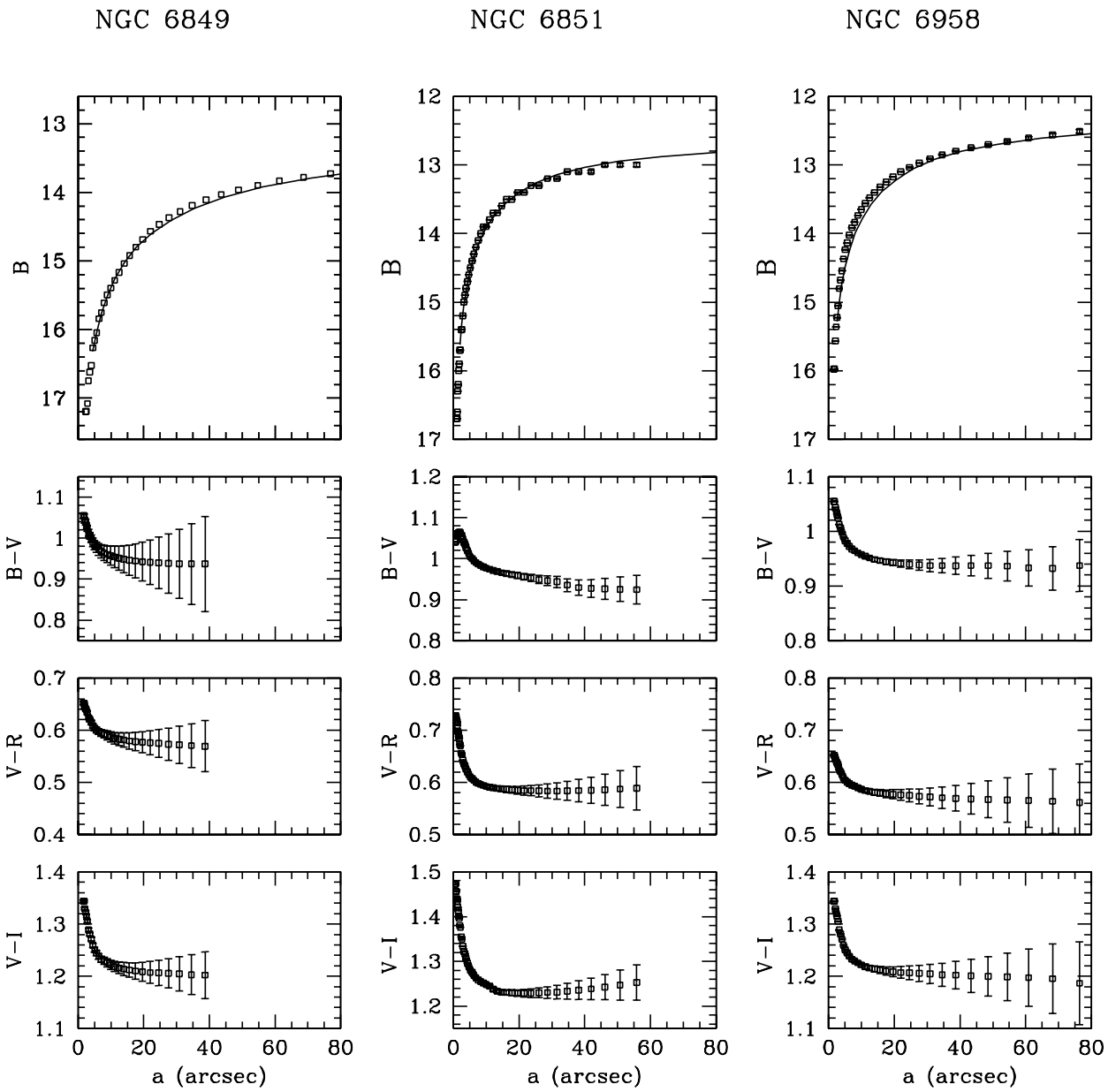

Fig. 8. Magnitudes and colors integrated in ellipses as a function of the semi-major axis of the ellipse. The standard growth curves that best fit the integrated magnitude curves are shown in the top panels as continuous lines.

4. Discussion

In this section we discuss the more interesting features of each galaxy separately and make comparisons among them.

NGC 6849: This elliptical galaxy is the flattest in our sample (ϵ = 0.36), and its isophotes are very pointed around $r = 35''$. This is probably the reason for its classification as barred in RC3. Nevertheless, the surface brightness profile can be well fitted by a one-component $r^{1/n}$ law, showing no indication of the presence of a bar, nor of a disk. The value that best describes the profile is $n = 2.4$, which means the profile is a little flatter than a de Vaucouleurs law. The B isophotes, in comparison with the other passbands, show stronger variations in ellipticity, in position angle and in deviations from elliptical shape, which might suggest the presence of dust or gas. The PA profile shows a total isophotal twist of $9°$. As the galaxy has no apparent companion this might be a hint of triaxiality. The color index profiles present a small blue gradient outwards, of almost 0.2 magnitudes in $V - I$. The integrated colors up to r = 40 $''$ are very similar to the colors of an elliptical galaxy of the spectral group E2 of Bica et al. (1990), corresponding to red nuclei of early-type galaxies of low luminosity.

NGC 6851: Surface photometry in the V and R filters was previously obtained by Toniazzo, Stiavelli & Zeilinger [1992 (TSZ)], and in the B, V, R, I filters by Sparks et al. (1991). The isophotal parameters in the present photometry are in agreement with the previous work, and show that this galaxy has disky and

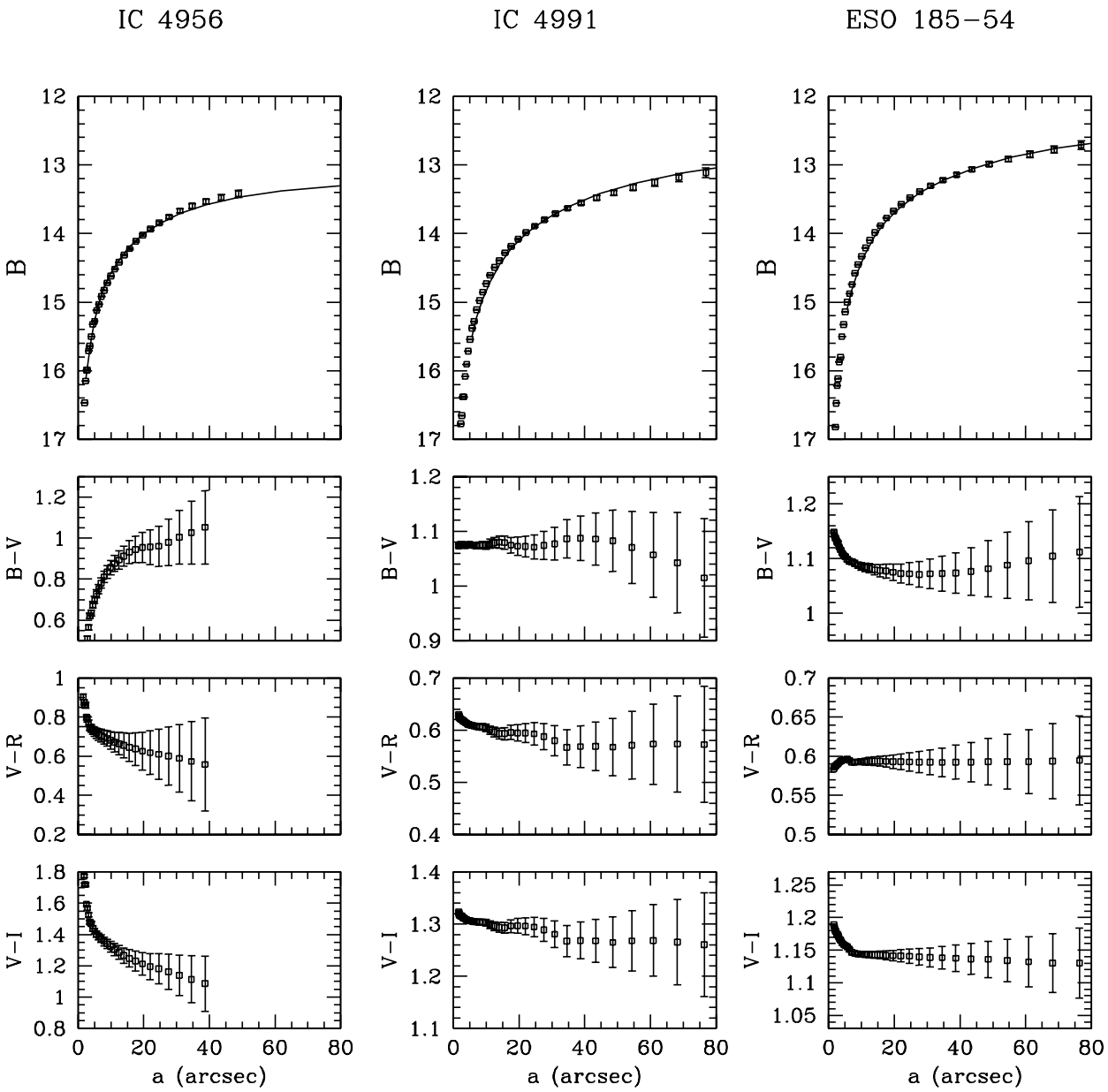

Fig. 8. (continued)

twisted isophotes. The diskiness of NGC 6851 is comparable to that of NGC 6849 ($B4 \simeq 0.02$), in fact these two galaxies are the most diskier in our sample, and the most elongated as well. But while NGC 6849 presents a moderate isophotal twist of less than 10°, the isophotes of NGC 6851 has a strong west-east twist of 30°. Twists this large are normally indicative of interaction. Although this galaxy has no apparent companion, it is classified as a member of a group with 5 galaxies by Maia, da Costa & Latham (1989). Another possibility for the origin of the twist is triaxiality, as already suggested by TSZ. In this galaxy the B isophotes behave differently than the other colors, but this difference is restricted to the nuclear region, where the B isophotes have greater ellipticity, are more pointy, and have different position angle. This may be associated with dust, and this hypothesis is supported by the very red nucleus. The luminosity profile is fitted by an $r^{1/5}$ law along the range of magnitudes $20 \leq \mu_B \leq 24$.

NGC 6958: This is the galaxy in our sample with more elliptical isophotes ($B4 \simeq 0$), and the one with the strongest isophotal twist, of almost 100° westward. It also has the more concave luminosity profile; the exponent of the Sersic law that best fits the profile is 6.8. These two last features could be explained by interaction. Nevertheless, the nearest galaxy in the field is a faint disk galaxy 320″ to the west that seems to be very farther away. If this galaxy suffered interaction, the companion galaxy is probably already merged. This possibility would be consistent with NGC 6958 being classified as a cD galaxy, believed to arise from galaxy mergers. The inconsistency is that this kind of

Table 6. Total magnitudes

Object	$B_{\rm T}{}^{\rm GC}$ $B_{\rm T}{}^{LP}$	Adopted $B_{\rm T}$ $(B_{\rm T})^0$	$m-M$	$M_{\rm T}(B)$ $M_{\rm T}(B)^0$
(1)	(2)	(3)	(4)	(5)
NGC 6849	13.32	13.31 ± 0.06	34.35	-21.04
	13.30	13.24 ± 0.06		-21.11
NGC 6851	12.65	12.66 ± 0.06	32.78	-20.10
	12.67	12.49 ± 0.06		-20.27
NGC 6958	12.28	12.28 ± 0.23	32.52	-20.24
	11.95	12.10 ± 0.23		-20.34
IC 4956	13.11	13.2 ± 0.16	33.99	-20.79
	13.30	13.1 ± 0.16		-20.89
IC 4991	12.51	12.6 ± 0.11	34.19	-21.59
	12.64	12.4 ± 0.11		-21.79
ESO 185-54	12.14	12.1 ± 0.16	33.58	-21.48
	12.11	12.0 ± 0.16		-21.58

Description of columns:
(1) name of the galaxy.
(2) total B magnitude derived from the standard growth curve (first line), and from the extrapolation of the luminosity profile using the fitted function (second line).
(3) adopted total B magnitude, as explained in Sect. 3.3 (first line), and total B magnitude corrected by galactic absorption (second line). The quoted uncertainties are the quadratic sum of the uncertainties in the mean of the two values in Column 1 and the errors in the integrated B magnitude as in Table 5.
(4) distance modulus, using the adopted distance in Table 1.
(5) absolute magnitude as observed (first line) and corrected by galactic absorption (second line)

galaxies are usually very luminous, whereas the distance modulus derived from the radial velocity of NGC 6958 indicates it has low luminosity (M_B = -20.24).

IC 4956: This face-on galaxy is the faintest in our sample, and the data has low signal-to-noise. This, added to the small ellipticity of the isophotes (between 0.1 and 0.15) results in a very large uncertainty in the position angle, and in a very strong twist of the isophotes. The best defined isophotal parameter is the $B4$ coefficient, that points to a disk shape for $7'' \leq r \leq 16''$. Although it is classified as elliptical, its luminosity profile cannot be fitted by a one component luminosity law. It is well fitted by a sum of a $r^{1/0.91}$ Sérsic law and an exponential disk, which in practice is equivalent to the sum of two exponentials. Thus the galaxy is better classified as an S0.

IC 4991: This SO galaxy is the most luminous in our sample, and the one with smallest color gradient. It has isophotal parameters similar to those of NGC 6958, in the sense that both galaxies have variations in ellipticity increasing outward accompanied by one directional isophotal twist (westward in both cases, but much smaller for IC 4991), and no significant deviations from elliptical shape. The light profile is well fitted by a Sersic $r^{1/6}$ law, but the fit is better with a combinations of a Sersic law and and exponential law.

ESO 185-54: This is the only galaxy in our sample with rectangular isophotes, and the only one in a rich field. It is also one of the galaxies with smallest isophotal twist. The position angle profiles has a big bump at $r \simeq 20''$, except in the I filter, that apparently is caused by masking a bright star at that position. As in the case of IC 4991, its color gradient is very small.

5. Conclusions

About the shape of the isophotes

All galaxies in our sample show some degree of twist in the position angle, varying from less than 10 to more than 90 degrees. The amount of twist is clearly anti-correlated with the maximum ellipticity, as previously noted by other authors (e.g. Benachio & Galleta 1980), and with the modulus of the $B4$ coefficient (the maximum ellipticity and the modulus of $B4$ *decrease* as the twist *increases*), and consequently the $B4$ modulus is correlated with the maximum ellipticity in the sense that the modulus of $B4$ *increases* as the maximum ellipticity *increases*. Since the maximum ellipticity depends on inclination, the deviation of ellipticity may be in part an effect of the inclination. However the sign of $B4$, that is, the kind of deviation from elliptical shape, has no correlation with the ellipticity. Thus it does not depend on inclination, and must therefore be an intrinsic characteristic of the galaxy.

Among our 6 galaxies, NGC 6849, NGC 6851, and ESO 185-54, have significant deviations from elliptical shape ($|B4| \geq 0.02$). The first two have disky isophotes, and the third, ESO 185-54, has very rectangular isophotes, and is the only object in our sample located in a rich field of galaxies. This is compatible with the suggestion by Bender & Möllenhoff (1987) that boxiness is probably the result of mergers of galaxies. On the other hand, the fact that it is also one of the galaxies with smaller twist implies that, either its boxiness did not originate in a merger event, or that mergers do not always cause rotation of the isophotes.

The isophotal parameters ellipticity, position angle and $B4$ do not vary significantly among the filters V, R, and I, but show a little different behavior in the B filter, probably associated to deviations caused by the presence of some dust or/and gas. The smaller signal-noise ratio of the B isophotes may also be contributing to this effect, when observed in the external isophotes.

About the shape of the luminosity profiles

The four elliptical galaxies, NGC 6849, NGC 6851, NGC 6958, and ESO 185-54, were fitted by a one-component $r^{1/n}$ Sersic law, with n varying between 2.4 and 7.0. The lenticular galaxies IC 4956 (previously classified as elliptical), and IC 4991, were best fitted by a combination of an $r^{1/n}$ and an exponential law, with n assuming the value 0.9 for one galaxy and 3.8 for the other. This confirms that while elliptical galaxies and bulges have brightness profiles that can be well described by a Sersic law (with shapes that can be more flattened of more curved than a de Vaucouleurs law), the brightness profiles of two component systems such as disk galaxies, cannot be well fitted by a Sersic law alone and require a two component model.

We did not find a unique correlation of the index n with the parameters r_e, μ_e and M_B. Our data seem to show two correlations, one valid for galaxies brighter, and other valid for the galaxies fainter than than M_B = 21, suggesting that the correlation depends on luminosity. However, the small number statistics do not really allow us to reach firmer conclusions.

About the colors

All the galaxies except IC 4956 show at least a small red gradient toward the nucleus, which could be an effect of age or metallicity. The gradient is very accentuated in NGC 6851, and in this galaxy it might be associated to the presence of dust.

The integrated and nuclear colors of the galaxies are typical of their morphological type, with no indication of significant events of star formation younger than one billion years in the nucleus. This discards the possibility of the presence of hot young stars there that could be ionizing the gas, and supports the hypothesis that post-AGB stars are responsible for the observed ionized hydrogen.

Acknowledgements. The authors are very grateful to the referee, Dr. Duccio Macchetto, for his very fruitful comments and suggestions. M.F. Saraiva also thanks Dr. Ronaldo de Souza, Dr. Eduardo Bica and Dr. S.O. Kepler for useful discussions, and Marcio Waterman and Rodrigo Ballejos for their help with the graphics. The authors acknowledge CNPq and PRONEX/FINEP 76.97.1003.00 for financial support.

References

Bender R., Möllenhoff C., 1987, A&A 177, 71
Benacchio L., Galleta G., 1980, MNRAS 193, 885
Bertola F., 1981, Sky Telesc., 61, 380
Bica E., Alloin D., Schmidt A., 1990, MNRAS 242, 241
Binney J., Petrou M., 1985. MNRAS 214, 449
Buta R., Willians K.L., 1995, AJ 109, 543
Caon N., Capaccioli M., D'Onofrio M., 1993, MNRAS 265, 1013
Capaccioli M., Caon N., 1991, MNRAS 248, 523
Capaccioli M., Longo G., 1994, A&AR 5, 293
Ciotti L., 1991, A&A 249, 99
da Costa L.N., Pellegrini P.S., Sargent W.L.W., et al., 1988, ApJ 327, 544
Ferrari F., Pastoriza M.G., Macchetto F.M., Caon N., 1999, A&A in press
Graham J.A., 1982, PASP 94, 244
Graham A., Lauer T., Colless M., Postman M., 1998, preprint
Goudfrooij P., Jong J., Jørgensen H.E., Nørgaard-Nielsen H.U., 1994, A&AS 105, 341
Hamabe M., Kormendy J., 1987, In: de Zeeuw P.T. (ed.) IAU Symp. 127, Reidel, Dordrecht, p. 379
Jedrzejewski R., Davies R., Illingworth G., 1987, AJ 94, 1508
Kormendy J., Djorgowsky S., 1989, ARA&A
Lauberts A., 1984, A&AS 58, 249
Longo G., de Vaucouleurs A., 1983, The University of Texas Monographs in Astronomy No. 3, Department of Astronomy, The University of Texas at Austin, Austin, Texas (LdV83)
Longo G., de Vaucouleurs A., 1985, The University of Texas Monographs in Astronomy No. 3A, Department of Astronomy, The University of Texas at Austin, Austin, Texas (LdV85)
Macchetto F., Pastoriza M., Caon N., et al., 1996, A&AS 120, 463
Maia M.A.G., da Costa L.N., Latham D.W., 1989, ApJS 69, 809
Mihalas D., Binney J., 1981, Galactic Astronomy (W.H. Freeman, São Francisco), p. 331
Persson S.E., Frogel J.A., Aaronson M., 1979, ApJS 39, 61
Poulain P., 1986, A&AS 64, 225
Poulain P., 1988, A&AS 72, 215
Poulain P., Nieto J.-L., 1994, A&AS 103, 573
Prugniel Ph., Simien F., 1997, A&A 321, 111
Prugniel Ph., Hérardeau Ph., 1998, A&AS 128, 299
Sadler E.M., 1984, AJ 89, 34
Sérsic J.L., 1968, Atlas de Galaxias Australes. Observatorio Astronomico, Cordoba, Argentina
Sparks W.B., Wall J.V., Jorden P.R., Thorne D.J., van Breda I., 1991, ApJS 76, 471
Tamman G.A., Sandage A., 1985, ApJ 294, 81dd
Toniazzo T., Stiavelli M., Zeilinger W.W., 1992, A&AS 259, 39